•水利与土木工程•

DOI:10.12454/j.jsuese.202300767

本刊网刊

三点弯曲下FRP板增强SHCC梁的剥离分析模型与试验研究

胡继洪,孙明清*,王应军,陈建中,黄　维

(武汉理工大学 新材料力学理论与应用湖北省重点实验室,湖北 武汉 430070)

摘　要:应变硬化水泥基复合材料(strain hardening cement-based composites,SHCC,也称ECC)在直拉和弯曲时呈现与普通混凝土不同的多条细裂纹依次开裂的力学特性,为研究外黏FRP板(采用玻璃纤维增强树脂制得)增强SHCC梁(简称FRP–SHCC梁)在弯曲承载时的剥离行为,开展了FRP–SHCC梁的弯曲试验与理论分析。基于SHCC分段刚度折减的方法量化SHCC细密裂纹对其与FRP板黏结应力的影响,提出一种先分段变刚度,再联合界面应力分析与截面力系平衡分析的求解方法:首先,将SHCC开裂后的FRP–SHCC梁分为弹性区和开裂区;然后,将开裂区细分成若干小段,假设开裂区梁段的抗弯刚度与压区高度从跨中到弹性区分段线性变化;随后,结合FRP板与SHCC界面的黏结应力–滑移关系、材料本构关系、梁横截面的静力平衡和FRP板的轴力控制微分方程等因素,得出各梁段FRP板的轴力和界面切应力的方程,并根据梁段边界条件和连续条件,采用MATLAB软件编程求解;最后,得出界面切应力、荷载–应变关系、荷载–挠度关系和FRP板剥离的起始位置等。结果表明:计算的FRP剥离起始点位置与试验观察位置基本一致,峰值荷载与试验值相比的偏差范围为–7.79%～7.45%,FRP应变与试验值相比的偏差范围为–11.52%～8.13%;在加载过程中,梁的荷载–挠度关系、荷载–应变关系的计算结果与试验结果基本吻合。本文研究可为此类新型复合土木工程结构的设计和弯曲行为分析提供参考。

关键词:FRP板增强SHCC梁;剥离;梁段;弯曲刚度;界面;黏结应力

中图分类号:TU398.9　　**文献标志码:**A　　**文章编号:**2096-3246(2025)04-0208-10

Li[1]、Fischer[2]和Yu[3]等采用的以PVA纤维和砂浆为主配制的应变硬化水泥基复合材料在拉伸时,产生了多条细裂纹,裂纹间距小于4 mm,细裂纹宽度一般小于100 μm,SHCC的极限拉伸应变超过3%,呈现应变硬化现象,具有较好的延性。Sui等[4]发现将SHCC层作为FRP板和普通混凝土间的过渡层使用时能延缓FRP的剥离,从而提高结构的承载力和延性。Maalej等[5]发现与无SHCC层的FRP增强普通钢筋混凝土(FRP–RC)梁相比,有SHCC层时裂纹两侧的界面切应力差异变小。Ferrari[6]、Afefy[7]等发现FRP–SHCC梁复合增强比FRP–RC梁的承载力分别增加65.1%和48.5%,复合梁最终的破坏模式是FRP的剥离,剥离起始于加载点旁约1倍梁高处。Zhou[8]、Hu[9]等的研究表明,单层FRP加固时,SHCC过渡层的加入使得梁的破坏由FRP剥离变为FRP断裂。除把SHCC作为过渡层使用外,关于FRP增强SHCC结构(无普通混凝土)也有一些报道[10–11],但有关FRP增强SHCC和FRP与SHCC复合增强钢筋混凝土梁基于跨中剥离失效的研究还较少,既有研究主要针对FRP–RC梁,其承载力的计算方法主要有以下3种:1)基于试验数据拟合的方法,Chen[12]和Teng[13]等基于试验数据拟合得到FRP–RC梁跨中FRP的剥离应变并求得FRP–RC梁的承载力,该方法已被ACI采纳[14],但该方法需要耗费大量人力和资源且周期较长;2)有限元方法,陆新征[15]采用精细有限元法,Cohen[16]和Al–Saawani[17]等采用牵引力分离法则模拟界面,用有限元法分别求得FRP–RC梁基于剥离破坏的承载力,但同时考虑混凝土开裂和界面剥离的建模比较复杂;3)解析与半解析方法,Teng等[18]以相邻裂纹间的梁段作为研究对象,将混凝土和FRP均看作弹性体,采用双线性黏结应力–滑移

收稿日期:2023 – 09 – 26　　**修回日期:**2023 – 12 – 24　　**网络出版日期:**2024 – 06 – 24

基金项目:国家自然科学基金青年项目(51608406);中央高校基本科研业务费专项资金(2021Ⅲ059JC)

作者简介:胡继洪(1976—),男,博士生. 研究方向:新材料与复合结构. E-mail:hujhll@sina.cn

* **通信作者:**孙明清,教授,E-mail: sunmqing@whut.edu.cn

关系，推导了不同受力状态梁段的界面切应力分布。Wang[19]将 FRP 和混凝土均视为弹性，将跨中裂纹等效为转动弹簧，将界面看作一个大尺度的断裂过程区，将非线性黏结应力–滑移关系作为界面内聚力法则，采用内聚区模型（cohesive zone model，CZM）定义界面，得到承载力的闭合解。Chen[20]和 Xu[21]等采用 Wang[19]方法分别对两个裂纹间的梁段和含多个裂纹的 FRP–RC 梁进行分析，获得不同阶段的界面应力分布。Slaitas 等[22]根据组合条理论，考虑界面滑移导致的整体构件刚度的降低，对 FRP 的应力进行折减，采用折减后的 FRP 应力计算梁的承载力，与试验吻合较好。Razaqpur 等[23]将弯矩–曲率随荷载变化的关系简化为三线性，并对应到 FRP–RC 梁的不同区域上，结合界面应力分析与截面力系平衡分析，求得 FRP 的应变分布，与试验结果基本吻合。Xie 等[24]基于断裂力学理论推导了界面裂纹能量释放率的计算公式，以界面断裂能作为剥离判据求得复合梁承载力预测公式，与试验结果吻合较好。方法 3）由于裂纹的随机性与界面的非线性，一般需要较多假设作为分析的前提，这些假设一般基于 FRP–RC 梁弯曲变形过程中的某些特征，与普通钢筋混凝土裂纹间距与 FRP 有效黏结长度接近不同，SHCC 的裂纹间距远小于 FRP 的有效黏结长度，此外 SHCC 的微裂纹能减小界面应力集中，因而 FRP–SHCC 梁的失效状态可能与 FRP–RC 梁不同，目前此类结构的试验和理论研究还较少。本文考虑将开裂后的 SHCC 梁沿轴向视为变刚度弹性体，把 SHCC 的抗弯刚度和复合梁压区高度沿梁轴向简化为线性分布，并分段取值，结合 FRP–SHCC 梁界面应力分析与横截面力系平衡条件，得到 FRP–SHCC 的界面切应力、FRP 拉应变、荷载–挠度关系等，并将计算结果与试验进行对比，这一研究将为类似结构的失效分析提供参考。

1　模型建立

1.1　基本假定

1）FRP 与 SHCC 弯曲时曲率相同。FRP 与 SHCC 曲率的差异是胶黏层沿厚度方向的变形不同导致的，由于胶黏层很薄，对比复合梁的曲率半径是相对小量；文献[19–21,23–24]采用此假定，计算结果与试验基本吻合，证明采用此假定对计算结果影响较小。

2）开裂 SHCC 梁符合平截面假定。平截面假定已被广泛应用于细长梁的分析，文献[25]基于此假定计算开裂 SHCC 梁的抗弯承载力，与试验吻合较好，本文考虑界面滑移，仅 SHCC 梁采用平截面假定是合适的。

3）忽略 FRP 与 SHCC 间界面正应力的影响。界面包含正应力和切应力，文献[26]的研究显示：裂纹嘴处存在正应力集中，但正应力传播速度较切应力快，在距离裂纹嘴很短的位置正应力即趋于 0，因而起控制作用的是切应力；文献[18–21,23–24]的研究显示，忽略其影响可以得到与试验接近的结果，此外，SHCC 的裂纹宽度较普通混凝土小，其正应力较普通混凝土的更小，其对计算结果的影响会更小，因而本文不考虑其影响。

1.2　材料的应力–应变关系

SHCC 压缩时的应力–应变曲线采用抛物线加水平直线[27]，SHCC 拉伸时的应力–应变曲线采用双线性[25]，如图 1 所示。

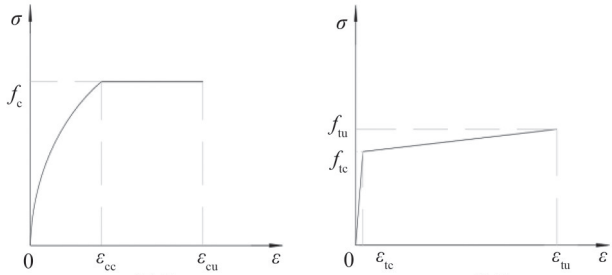

(a) 压缩[27]　　(b) 拉伸[25]

图 1　SHCC 的应力–应变曲线

Fig. 1　Stress–strain curves of SHCC

图 1 中，σ 为应力，ε 为应变，f_c 为 SHCC 的压缩强度，ε_{cc}、ε_{cu} 分别为 SHCC 刚达到抗压强度时的压应变和极限压应变，f_{tc}、f_{tu} 分别为 SHCC 初裂拉伸应力和拉伸强度，ε_{tc}、ε_{tu} 分别为 f_{tc} 和 f_{tu} 对应的应变。

SHCC 压缩和拉伸时的应力–应变关系分别表示如下：

$$\sigma_c=\begin{cases} f_c\left[2\dfrac{\varepsilon}{\varepsilon_{cc}}-\left(\dfrac{\varepsilon}{\varepsilon_{cc}}\right)^2\right], 0<\varepsilon\le\varepsilon_{cc}; \\ f_c, \varepsilon_{cc}<\varepsilon\le\varepsilon_{cu} \end{cases} \tag{1}$$

$$\sigma_t=\begin{cases} \dfrac{f_{tc}}{\varepsilon_{tc}}\varepsilon, 0<\varepsilon\le\varepsilon_{tc}; \\ f_{tc}+\dfrac{f_{tu}-f_{tc}}{\varepsilon_{tu}-\varepsilon_{tc}}\left(\varepsilon-\varepsilon_{tc}\right), \varepsilon_{tc}<\varepsilon\le\varepsilon_{tu} \end{cases} \tag{2}$$

式（1）～（2）中，σ_c、σ_t 分别表示 SHCC 压应力和拉应力。

FRP 采用弹脆性本构，如下所示：

$$\sigma_f=\begin{cases} E_f\varepsilon, 0\le\varepsilon\le\varepsilon_{fu}; \\ 0, \varepsilon>\varepsilon_{fu} \end{cases} \tag{3}$$

式中，σ_f 为 FRP 拉应力，E_f、ε_{fu} 分别为 FRP 的弹性模量和断裂应变。

1.3　界面黏结应力–滑移关系

与普通混凝土相比，SHCC 的特点是开裂后，纤维在裂纹间产生的桥联应力使得构件具备高延性，其他力学性能与混凝土类似，因而裂纹间的界面黏结应力–滑移关系可以参考普通混凝土的相关研究。本文后续

试验也显示FRP–SHCC界面黏结应力–滑移关系曲线与FRP–RC的形状类似，只是参数不同。

参考陆新征[15]的研究，为便于分析，本文将上升段简化为线性，其表达式如下：

$$\tau=\begin{cases}\dfrac{\tau_m}{\delta_0}\delta, & 0\le\delta\le\delta_0;\\ 0, & \delta>\delta_0\end{cases} \tag{4}$$

式中，δ为界面滑移，τ为界面切应力，τ_m为峰值切应力，δ_0为τ_m对应的界面局部滑移。

简化的界面黏结应力–滑移关系曲线如图2所示。

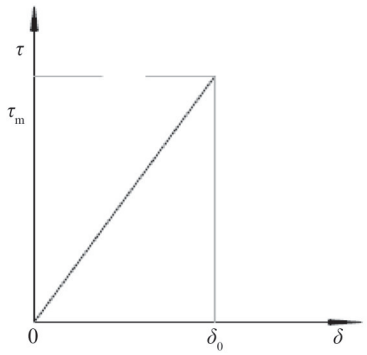

图2 FRP–SHCC界面黏结应力–滑移关系曲线

Fig. 2 FRP–SHCC interface bond stress–slip relationship curve

1.4 模型建立

以跨中集中力作用下的FRP–SHCC简支梁为研究对象，如图3所示。图3中：F为荷载；h为复合梁高度，$h=t_f+h_c$，t_f和h_c分别为FRP板和SHCC梁的高度。由于对称，可取梁的1/2进行分析，取界面中点为坐标原点。

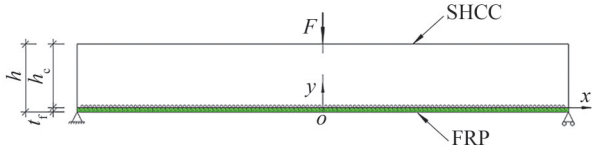

图3 跨中集中力作用下的FRP–SHCC简支梁

Fig. 3 Simply supported FRP–SHCC beam under three-point bending

1.4.1 弹性阶段

将半跨梁作为一个梁段，取微段进行分析，受力如图4所示。

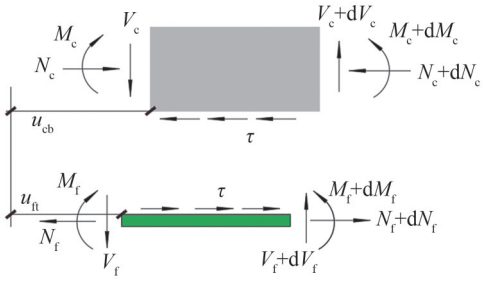

图4 梁微段受力图

Fig. 4 Force diagram of the beam element

图4中，N_f、N_c分别为FRP和SHCC的轴力，M_f、M_c分别为FRP和SHCC的弯矩，V_f、V_c分别为FRP和SHCC的剪力，u_{ft}为FRP顶部的位移，u_{cb}为SHCC底部的位移。

由力系平衡可得：

$$\frac{dN_f}{dx}=-b_f\tau \tag{5}$$

$$M=M_c+M_f+N_f\left(\frac{h_c}{2}+\frac{t_f}{2}\right) \tag{6}$$

式(5)～(6)中，M为复合梁横截面上承担的弯矩，b_f为FRP的宽度。

FRP与SHCC界面间滑移δ为u_{ft}和u_{cb}之差，即：

$$\delta=u_{cb}-u_{ft} \tag{7}$$

代入式(4)可得：

$$\tau=\frac{\tau_m}{\delta_0}(u_{cb}-u_{ft}) \tag{8}$$

对式(8)求导1次可得：

$$\frac{d\tau}{dx}=\frac{\tau_m}{\delta_0}(\varepsilon_{cb}-\varepsilon_{ft}) \tag{9}$$

式中，ε_{cb}和ε_{ft}分别为SHCC底部的应变和FRP顶部的应变，二者之差即为界面滑移应变ε_s。ε_{cb}和ε_{ft}分别由下式求得：

$$\varepsilon_{cb}=-\frac{N_c}{C_c}+\frac{M_c}{D_c}\cdot\frac{h_c}{2} \tag{10}$$

$$\varepsilon_{ft}=\frac{N_f}{C_f}-\frac{M_f}{D_f}\cdot\frac{t_f}{2} \tag{11}$$

式(10)～(11)中，C_f、C_c分别为FRP和SHCC的拉压刚度，D_f、D_c分别为FRP和SHCC的抗弯刚度。

将式(10)和(11)代入式(9)可得：

$$\frac{d^2N_f}{dx^2}=-b_f\frac{\tau_m}{\delta_0}\left(\frac{h_c}{2}\cdot\frac{M_c}{D_c}-\frac{N_c}{C_c}-\frac{N_f}{C_f}+\frac{t_f}{2}\cdot\frac{M_f}{D_f}\right) \tag{12}$$

由FRP与SHCC曲率相等的假设和式(6)得：

$$\frac{M_c}{D_c}=\frac{M_f}{D_f}=\frac{M_c+M_f}{D_c+D_f}=\frac{M-N_f\left(\frac{h_c}{2}+\frac{t_f}{2}\right)}{D_c+D_f} \tag{13}$$

将式(13)代入式(12)，整理得FRP轴力的控制微分方程：

$$\frac{d^2N_f}{dx^2}-\lambda_0^2N_f=-\lambda_0^2C_\tau M \tag{14}$$

式中，

$$\lambda_0=\sqrt{b_f\frac{\tau_m}{\delta_0}\left[\frac{1}{C_f}+\frac{1}{C_c}+\frac{\left(\frac{h_c}{2}+\frac{t_f}{2}\right)^2}{D_c+D_f}\right]} \tag{15}$$

$$C_\tau=\frac{\frac{h_c}{2}+\frac{t_f}{2}}{(D_c+D_f)\left[\frac{1}{C_f}+\frac{1}{C_c}+\frac{\left(\frac{h_c}{2}+\frac{t_f}{2}\right)^2}{D_c+D_f}\right]} \tag{16}$$

式(14)的解为：

$$N_{\mathrm{f}}=C_1\mathrm{e}^{-\lambda_0 x}+C_2\mathrm{e}^{\lambda_0 x}+C_\tau M \tag{17}$$

式中，C_1、C_2 为常系数。对式(17)求导 1 次可得界面切应力：

$$\tau=-\frac{1}{b_{\mathrm{f}}}(-\lambda_0 C_1\mathrm{e}^{-\lambda_0 x}+\lambda_0 C_2\mathrm{e}^{\lambda_0 x}+C_\tau\frac{\mathrm{d}M}{\mathrm{d}x}) \tag{18}$$

将式(18)代入式(9)可得界面滑移应变：

$$\varepsilon_{\mathrm{s}}=-\frac{\delta_0}{\tau_{\mathrm{m}}}\cdot\frac{1}{b_{\mathrm{f}}}(\lambda_0^2 C_1\mathrm{e}^{-\lambda_0 x}+\lambda_0^2 C_2\mathrm{e}^{\lambda_0 x}+C_\tau\frac{\mathrm{d}^2M}{\mathrm{d}x^2}) \tag{19}$$

常系数 C_1、C_2 根据边界条件 $\tau|_{x=0}=0$ 和 $N_{\mathrm{f}}|_{x=\frac{L}{2}}=0$ 求得：

$$\begin{cases} C_1=-\dfrac{1}{2}\cdot\dfrac{C_\tau}{\lambda_0}\cdot\dfrac{\mathrm{e}^{\lambda_0 L}}{\mathrm{e}^{\lambda_0 L}+1}F, \\ C_2=\dfrac{1}{2}\cdot\dfrac{C_\tau}{\lambda_0}\cdot\dfrac{1}{\mathrm{e}^{\lambda_0 L}+1}F \end{cases} \tag{20}$$

1.4.2　开裂阶段

SHCC 开裂后，将梁分为开裂区(细裂纹分布区)和弹性区。随荷载增加开裂区不断扩大，开裂区与弹性区分界点(以下简称为分界点)逐渐往支座移动。在弹性区，FRP 的轴力控制微分方程为式(14)。对于开裂区，将其分为若干小段，并假设 SHCC 的等效抗弯刚度和压区高度(即 FRP–SHCC)梁的中性轴到梁顶部的距离)从分界点到跨中按线性变化。由于跨中加载点处 SHCC 内的应力存在扩散现象，扩散角接近 45°[28]，如图 5 所示。

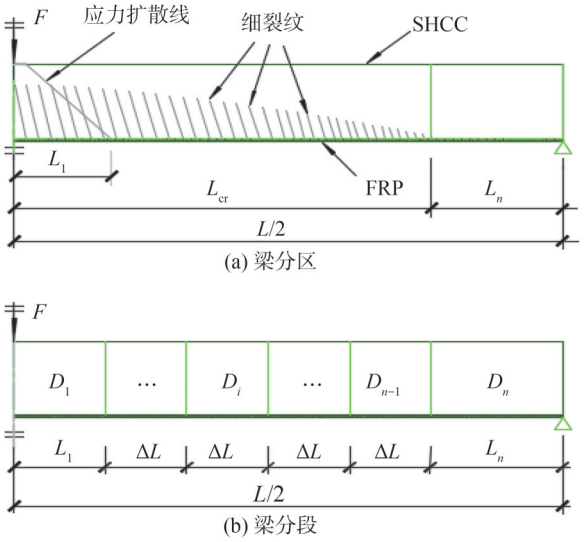

图 5　梁分区与分段示意图

Fig. 5　Systematic diagram of segments of the beam

图 5 中，L 为跨长，L_{cr} 为开裂区长度，L_n 为弹性段长度，D_i 为第 i 个开裂梁段 SHCC 的等效抗弯刚度(用各段中点所对应的值表示)，D_1 为应力扩散段 SHCC 的抗弯刚度(即跨中处)，D_n 为分界点处 SHCC 的抗弯刚度，以同样的方法定义压区高度。

从图 5 中可以看出，从跨中开始取长度相当于 SHCC 高度的梁段作为应力扩散段 L_1，开裂区的其余部分按等长分段(每段长 ΔL)，选取不同的 ΔL 计算界面切应力，当界面最大切应力随 ΔL 变化而改变不大时，即确定 ΔL 的大小。

按上一段的假设，可得各梁段的抗弯刚度和压区高度的表达式：

$$\begin{cases} D_i=D_n-\dfrac{D_n-D_1}{\dfrac{L}{2}-L_1-L_n}(i-1/2)\Delta L, \\ y_i=y_n-\dfrac{y_n-y_1}{\dfrac{L}{2}-L_1-L_n}(i-1/2)\Delta L \end{cases} \tag{21}$$

式中，y_i 为第 i 梁段中点截面的压区高度，y_1 为跨中截面的压区高度，y_n 为分界点处截面的压区高度。

以第 i 梁段为例求 FRP 的轴力与界面切应力。根据弯矩–刚度–曲率的关系，梁段中的 $\varepsilon_{\mathrm{cb}}$ 可近似由式(22)求得：

$$\varepsilon_{\mathrm{cb}}=\frac{M_{\mathrm{c}}}{D_i}(h_{\mathrm{c}}-y_i) \tag{22}$$

同第 1.4.1 节分析方法可得：

$$\frac{\mathrm{d}^2N_{\mathrm{f}}}{\mathrm{d}x}=-b_{\mathrm{f}}\frac{\tau_{\mathrm{m}}}{\delta_0}[\frac{M_{\mathrm{c}}}{D_i}(h_{\mathrm{c}}-y_i)-(\frac{N_{\mathrm{f}}}{C_{\mathrm{f}}}-\frac{M_{\mathrm{f}}}{D_{\mathrm{f}}}\cdot\frac{t_{\mathrm{f}}}{2})] \tag{23}$$

整理后得：

$$\frac{\mathrm{d}^2N_{\mathrm{f}}}{\mathrm{d}x^2}-\lambda_i^2N_{\mathrm{f}}=-\lambda_i^2C_{\tau i}M \tag{24}$$

式中：

$$\lambda_i=\sqrt{b_{\mathrm{f}}\frac{\tau_{\mathrm{m}}}{\delta_0}(\frac{1}{C_{\mathrm{f}}}+\frac{(h-y_i+\frac{t_{\mathrm{f}}}{2})^2}{D_i+D_{\mathrm{f}}})} \tag{25}$$

$$C_{\tau i}=\frac{h-y_i+\frac{t_{\mathrm{f}}}{2}}{D_i+D_{\mathrm{f}}}/(\frac{1}{C_{\mathrm{f}}}+\frac{(h-y_i+\frac{t_{\mathrm{f}}}{2})^2}{D_i+D_{\mathrm{f}}}) \tag{26}$$

第 i 梁段中 FRP 的轴力与界面切应力为：

$$\begin{cases} N_{\mathrm{f}i}=C_{1i}\mathrm{e}^{-\lambda_i x}+C_{2i}\mathrm{e}^{\lambda_i x}+C_{\tau i}M, \\ \tau_i=-\dfrac{1}{b_{\mathrm{f}}}[\lambda_i(-C_{1i}\mathrm{e}^{-\lambda_i x}+C_{2i}\mathrm{e}^{\lambda_i x})+C_{\tau i}\dfrac{\mathrm{d}M}{\mathrm{d}x}] \end{cases} \tag{27}$$

式中，C_{1i}、C_{2i} 为常系数。共计 $2n$ 个(n 指图 5 中的总分段数)，需要建立 $2n$ 个方程，由边界条件和连续条件可得：

$$\begin{cases} \tau_{\mathrm{f}1}^-=0, \\ \quad\vdots \\ N_{\mathrm{f}i}^+=N_{\mathrm{f}i+1}^-, \\ \tau_{\mathrm{f}i}^+=\tau_{\mathrm{f}i+1}^-, \\ \quad\vdots \\ N_{\mathrm{f}n}^+=0 \end{cases} \tag{28}$$

式中，第 1 个式子表示跨中点界面切应力为 0，最后 1 个式子表示板端 FRP 轴力为 0，其他方程由连续条件(FRP 的轴力与界面切应力在分段处相等)得到，上标 –、+分别表示梁段的左端和右端截面。

1.5 求解步骤

1)输入荷载F,设置荷载增量Δx,由式(15)～(20)求弹性阶段界面切应力$\tau(x)$与FRP轴力$N_{\mathrm{f}}(x)$。

2)由求得的FRP的轴力,确定式(29)所示的静力平衡方程:

$$\begin{cases}\displaystyle\int_0^{y^{\mathrm{c}}}\sigma(y)b_{\mathrm{c}}\mathrm{d}y=\int_0^{h-y^{\mathrm{c}}-t_{\mathrm{f}}}\sigma(y)b_{\mathrm{c}}\mathrm{d}y+N_{\mathrm{f}},\\ \displaystyle\int_0^{y^{\mathrm{c}}}\sigma(y)b_{\mathrm{c}}y\mathrm{d}y+\int_0^{h-y^{\mathrm{c}}-t_{\mathrm{f}}}\sigma(y)b_{\mathrm{c}}y\mathrm{d}y+N_{\mathrm{f}}(h-y^{\mathrm{c}}-t_{\mathrm{f}})=M\end{cases}\tag{29}$$

式中,$\sigma(y)$为SHCC横截面上的应力,y^{c}为压区高度。

由式(1)和(2)得到跨正中SHCC底部的应变$\varepsilon_{\mathrm{cb}}$,当$\varepsilon_{\mathrm{cb}}\geq\varepsilon_{\mathrm{tc}}$时,进入SHCC开裂阶段。

3)SHCC开裂后,在式(19)求得的跨中界面滑移应变上增加$\Delta\varepsilon_{\mathrm{s}}$,定义为$\varepsilon_{\mathrm{s}}^{\mathrm{m}}$,并按式(29)求得跨中梁截面的应变分布与压区高度y_1,再由式(30)求D_1:

$$D_1=\frac{M_{\mathrm{c}}\big|_{x=0}}{\varphi_1}=\frac{M_{\mathrm{c}}\big|_{x=0}y_1}{\varepsilon_{\mathrm{c1}}}\tag{30}$$

式中,φ_1为跨中梁的截面曲率,$\varepsilon_{\mathrm{c1}}$为跨中SHCC顶部的压应变,$M_{\mathrm{c}}\big|_{x=0}$为跨中SHCC承受的弯矩。

4)假定分界点位置为x,则可求得分界点处的弯矩,取分界点处SHCC底部的应变为$\varepsilon_{\mathrm{tc}}$,由分界点处静力平衡可得横截面上的应力应变分布、抗弯刚度D_n和压区高度y_n。

5)当开裂区长度小于L_1时,将梁分为2段;当开裂区长度大于L_1时,按第1.4.2节要求分段。

由式(21)分别求各梁段SHCC抗弯刚度D_i和压区高度y_i。当分界点在FRP截断点与支座间时,直接由式(29)求得截面应力应变分布及压区高度,由式(30)求得该截面弯曲刚度,并替换弹性梁段弯曲刚度与压区高度按式(21)进行分段。

6)由式(27)和(28)求得各梁段N_{fi}和τ_i。

7)由式(27)和(28)求分界点处FRP的轴力N_{fn}^{+},根据静力平衡计算SHCC拉区应变,比较与初裂应变的差异是否小于设定值,否则在步骤4)的基础上增加Δx,从此步开始重新计算。

8)比较由式(27)和(28)求得的跨中FRP的轴力N_{fl}^{-}与式(29)求得的跨中FRP的轴力N_{fl}^{-}的差异是否小于设定值,否则在步骤3)的基础上增加一个$\Delta\varepsilon_{\mathrm{s}}$,由步骤3)开始重新计算。

9)按式(31)计算跨中挠度w[25]:

$$w=\varphi_1L^2/8\tag{31}$$

10)校核是否有梁段界面切应力τ_i达到了峰值τ_{m},否则增加一个ΔF,从步骤3)开始重复上述过程。

采用Matlab软件编程求解。

2 试验与计算结果对比

FRP–SHCC梁长400 mm,宽50 mm,高分别为32和48 mm。SHCC和FRP材料参数见表1[11,29]。FRP板宽为50 mm,厚分别为2.5、3.5、4.0、4.5和5.5 mm。在FRP板表面黏砂后,再在其上浇筑SHCC浆体制得FRP–SHCC梁。以试样代号F5.5–S48为例,其含义为:F5.5表示FRP厚为5.5 mm,S48表示复合梁高为48 mm。采用三点弯曲试验,跨度为350 mm。在FRP板底部以跨中点为中心,均匀粘贴7个应变片,应变片间距为20 mm。加载设备为INSTRON 5882,位移控制加载,速率0.4 mm/min。试样制备和试验过程详见文献[11]。

表1 FRP和SHCC的力学性能[11,29]

Tab. 1 Mechanical properties of FRP and SHCC[11,29]

E_{f}/GPa	E_{c}/GPa	f_{cu}/MPa	$\varepsilon_{\mathrm{ce}}$	$\varepsilon_{\mathrm{cu}}$	f_{tc}/MPa	f_{tu}/MPa	$\varepsilon_{\mathrm{tu}}$
23.5	16.3	34.5	0.004	0.005 5	2.6	4.5	0.04

注:E_{c}为SHCC的弹性模量,f_{c}为SHCC的抗压强度。

界面黏结–滑移关系由单面剪切试验获得。试样制作同FRP–SHCC梁,如图6所示,SHCC为75 mm×75 mm×300 mm的棱柱体,FRP板尺寸为500 mm×25 mm×4 mm。根据文献[15,30]的研究,界面黏结应力峰值及其对应的滑移与FRP板厚无关,因而试验选用中间厚度的FRP板(4 mm)。在FRP板的暴露面沿轴向粘贴10个应变片(图6中S1～S10)。测试时,SHCC棱柱体的上端固定,拉力作用在FRP板外伸端。由测量的各处FRP应变差分求得界面切应力。假定FRP自由

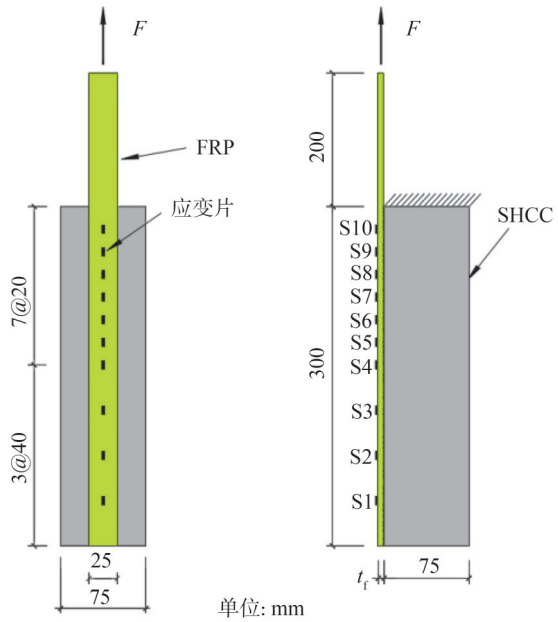

图6 FRP–SHCC梁单面剪切试验

Fig. 6 Interfacial shear test between FRP and SHCC

端的应变为 0，根据应变积分求得界面滑移[30]。共测试了 4 个试样，取平均值得：峰值界面切应力 $\tau_m=3.0$ MPa，对应滑移 $\delta_0=0.08$ mm。典型的界面黏结应力–滑移关系如图 7 所示。由图 7 可知，单剪状态下界面黏结–滑移关系曲线包含上升支和下降支，但陆新征[15]根据精细有限元法对单剪和弯曲下的界面黏结–滑移关系进行对比分析，认为复合梁在弯曲时，靠近混凝土主裂纹区域的界面切应力达到峰值后会出现陡降，据此提出近裂纹剥离准则，进一步研究显示，全梁采用此准则，分析结果仅比试验结果小 3.7%，因而全梁可以统一采用近裂纹准则来模拟，该界面黏结–滑移关系的上升段为曲线，切应力达到峰值后陡降至 0。本文为分析方便采用线性界面黏结–滑移关系。

FRP–SHCC 梁的弯曲试验与计算结果如表 2 所示。由表 2 可见，峰值荷载的计算值与试验值相比的偏差范围为–7.79%～7.45%，FRP 板应变的计算值与试验值相比的偏差范围为–11.52%～8.13%，分析结果与试验结果吻合较好。由于分析过程类似，以下以试样 F5.5–S48 为例说明分析过程。计算结果显示，加载至弹性极限荷载 0.64 kN 时，FRP 的拉应变较小，应变从跨中往支座方向接近线性减小。随荷载增加，跨中 SHCC 开裂，FRP 的应变明显增加。荷载为 5 kN 时，有关的中间计算参数为：弹性区长度（均对半跨梁而言，下同）为 39 mm，开裂区长度为 136 mm。开裂区中，应力扩散段长为 48 mm，开裂区的其余部分被分为 3 段，每段长 29.2 mm。此时计算的跨中 SHCC 弯曲刚度约为分界点处的 0.52 倍，跨中 SHCC 压区高度约为起裂点的 0.84 倍。当荷载达到 10.58 kN（峰值荷载）时，弹性段长度减小为 19.6 mm，半跨梁内开裂区域为 155.4 mm，取应力扩散段长为 48 mm，其余开裂梁部分分为 4 段进行计算，每段长 26.7 mm，跨中 SHCC 弯曲刚度为起裂点处的 0.38 倍，跨中 SHCC 压区高度约为起裂点处的 0.80 倍。F5.5–S48 梁加载过程中的 FRP 的应变分布如图 8 所示。由图 8 可知，计算得到的应变分布与试验基本吻合。

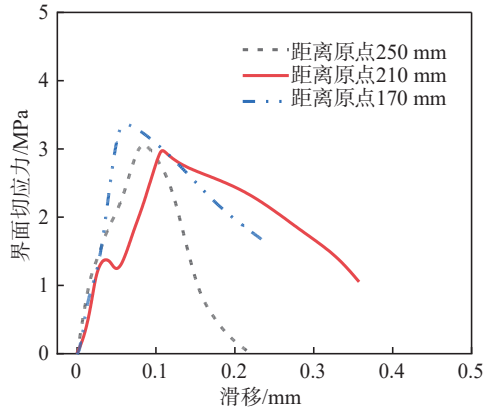

图 7　FRP–SHCC 界面黏结应力–滑移关系曲线

Fig. 7　Interfacial bond stress-slip curve of FRP and SHCC

表 2　FRP–SHCC 梁的弯曲试验和计算结果

Tab. 2　Bending expeiment and calculation results of FRP–SHCC beams

试样编号	试验		计算			
	峰值荷载/kN	峰值荷载对应的跨中应变	峰值荷载/kN	偏差/%	峰值荷载对应的跨中应变	偏差/%
F2.5–S48	10.07	0.005 067	9.90	–1.69	0.005 479	8.13
F3.5–S48	11.00	0.004 699	10.40	–5.45	0.004 322	–8.02
F4.0–S48	10.72	0.003 972	10.50	–2.05	0.003 901	–1.79
F4.5–S48	11.43	0.003 599	10.54	–7.79	0.003 556	–1.21
F5.5–S48	11.45	0.003 098	10.58	–7.60	0.003 035	–2.04
F4.0–S32	5.77	0.004 688	6.20	7.45	0.004 148	–11.52

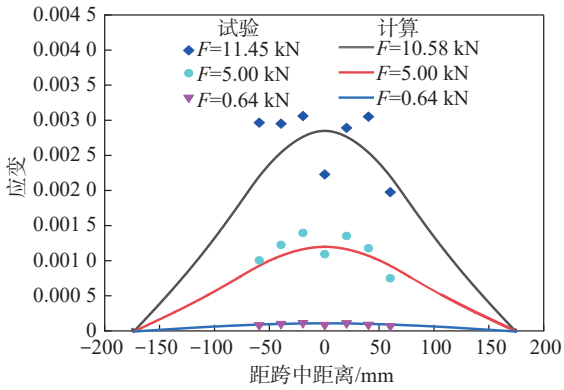

图 8　F5.5–S48 梁加载过程中 FRP 的应变分布

Fig. 8　Strain distribution of FRP plate of F5.5–S48

F5.5–S48 梁加载过程中的界面切应力分布如图 9 所示。由图 9 可知：弹性极限荷载（0.64 kN）时，界面切应力在支座附近最大，约为 0.11 MPa，由支座往跨中逐渐减小至 0。SHCC 开裂后，界面切应力从跨中点开始增加，在应力扩散段边缘附近，界面切应力达到最大，然后又减小。当荷载为 5 kN 时，界面切应力最大值为 1.17 MPa。当荷载增加到 10.58 kN 时，在应力扩散段边缘界面切应力达到峰值，FRP 板在此处发生剥离。数码相机拍摄的 FRP 板剥离破坏后的照片如图 10 所示。图 10 中，白色的箭头表示 FRP 板剥离发生的起始位置，大致位于应力扩散段边缘附近，与计算结果比

较一致。需要指出的是，模型是理想化的，对称结构的分析结果会呈对称分布，但试件制作不可避免存在局部偏差，导致 FRP 的剥离总是出现在较弱的一边，以致试验破坏出现非对称现象。

图 11 为各梁的荷载–跨中挠度关系曲线。

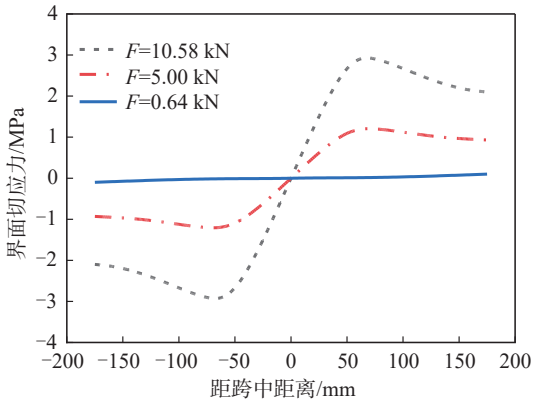

图 9 F5.5–S48 梁加载过程中界面切应力分布

Fig. 9 Interfacial shear stress along FRP and SHCC interface of F5.5–S48

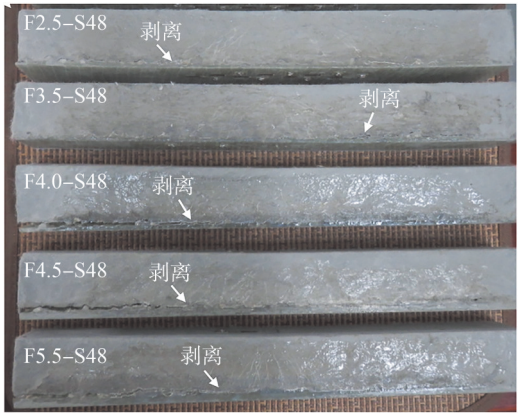

图 10 FRP–SHCC 梁的 FRP 板剥离破坏后现象

Fig. 10 Phenomenon after FRP plate debonding from SHCC beam

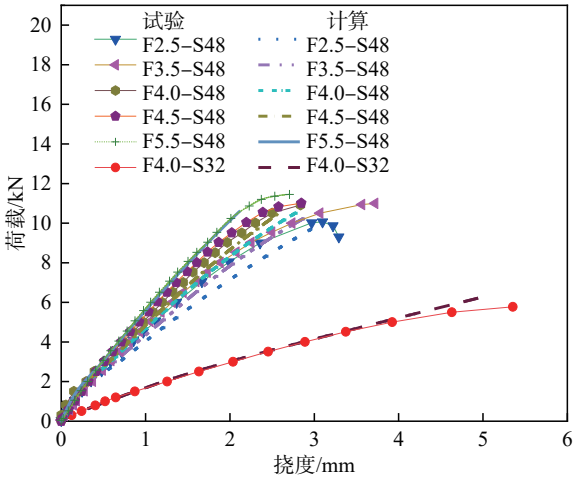

图 11 FRP–SHCC 梁的荷载–跨中挠度关系

Fig 11 Relation between load and deflection at the mid-span of FRP–SHCC beams

由图 11 可知，各梁变形过程类似，弹性阶段较短，随荷载增加，曲线斜率逐渐减小，说明随着 SHCC 裂纹的萌生和发展，复合梁刚度逐渐减小。除接近剥离时的一小段外，跨中挠度的计算结果与试验结果吻合较好。试验中，在接近峰值荷载时，荷载–挠度曲线的斜率逐渐减小至接近 0，说明界面出现微观剥离，可能本文采用的线性界面黏结应力–滑移关系还不能模拟这个过程，这个问题还需要进一步研究。

图 12 为荷载–跨中 FRP 应变关系曲线。由图 12 可见，FRP 应变在 SHCC 刚开裂时明显向横轴偏转，之后则逐渐接近线性增加，随 FRP 板厚增加曲线斜率增大。计算结果与试验基本吻合。

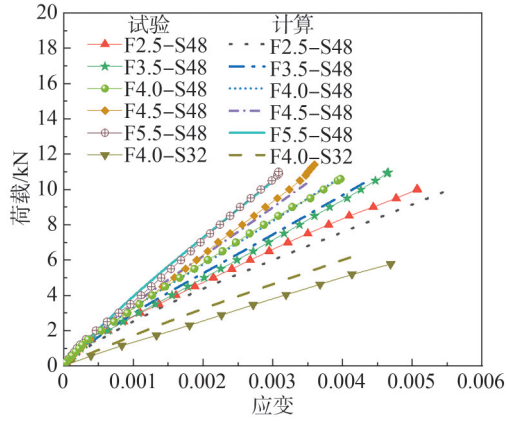

图 12 FRP–SHCC 梁的荷载–跨中 FRP 应变关系

Fig 12 Relation between load and strain at the mid-span of FRP–SHCC beams

3 结 论

1）针对 SHCC 多条细裂纹依次开裂的特点，建立分析 FRP 板增强 SHCC 梁基于剥离失效的力学模型，将开裂区 SHCC 的抗弯刚度和压区高度分段线性取值，得出复合梁在弯曲下的力学响应。峰值荷载的计算值与试验值相比的偏差范围为–7.79%～7.45%，跨中 FRP 应变的计算值与试验值相比的偏差范围为–11.52%～8.13%。在加载全过程中，梁的荷载–挠度关系、荷载–FRP 跨中应变的计算结果与试验基本吻合。

2）SHCC 开裂前的界面切应力由跨中往板端逐渐增加，SHCC 开裂后的界面切应力由跨中往板端先增大后减小，界面切应力峰值在应力扩散段边缘附近，此处为 FRP 剥离的起始位置，与试验观察到的剥离起始位置一致。

3）本文采用对开裂 SHCC 梁分段刚度折减的方法来量化 SHCC 不同区域的裂纹扩展程度对界面黏结应力的影响，同时考虑界面滑移对 FRP 增强 SHCC 梁进行剥离失效分析，结果与试验基本吻合，可以作为类似结构分析的参考。

本文对开裂SHCC梁的抗弯刚度和压区高度分段线性取值，与实际存在差异，寻找更接近实际的抗弯刚度与压区高度分布曲线进行分析是下一步需要开展的工作；此外还需要采用精细的界面黏结应力–滑移关系对剥离全过程深入分析。

参考文献：

[1] Li V C, Leung C K Y. Steady-state and multiple cracking of short random fiber composites[J]. Journal of Engineering Mechanics, 1992, 118(11): 2246–2264.

[2] Fischer G, Li V C. Effect of fiber reinforcement on the response of structural members[J]. Engineering Fracture Mechanics, 2007, 74(1/2): 258–272.

[3] Yu Kequan, Wang Yichao, Yu Jiangtao, et al. A strain-hardening cementitious composites with the tensile capacity up to 8% [J]. Construction and Building Materials, 2017, 137: 410–419.

[4] Sui Lili, Luo Minshen, Yu Kequan, et al. Effect of engineered cementitious composite on the bond behavior between fiber-reinforced polymer and concrete[J]. Composite Structures, 2018, 184: 775–788.

[5] Maalej M, Leong K S. Engineered cementitious composites for effective FRP-strengthening of RC beams[J]. Composites Science and Technology, 2005, 65(7/8): 1120–1128.

[6] Ferrari V J, de Hanai J B, de Souza R A. Flexural strengthening of reinforcement concrete beams using high performance fiber reinforcement cement-based composite(HPFRCC) and carbon fiber reinforced polymers(CFRP)[J]. Construction and Building Materials, 2013, 48: 485–498.

[7] Afefy H M, Kassem N, Hussein M. Enhancement of flexural behaviour of CFRP-strengthened reinforced concrete beams using engineered cementitious composites transition layer[J]. Structure and Infrastructure Engineering, 2015, 11(8): 1042–1053.

[8] Zhou Yingwu, Sui Lili, Huang Xiaoxu, et al. Enhancing the EB-FRP strengthening effectiveness by incorporating a cracking-control layer of ECC with different thicknesses [J]. Construction and Building Materials, 2021, 286: 122975.

[9] Hu Biao, Zhou Yingwu, Xing Feng, et al. Experimental and theoretical investigation on the hybrid CFRP-ECC flexural strengthening of RC beams with corroded longitudinal reinforcement[J]. Engineering Structures, 2019, 200: 109717.

[10] Hu Jihong, Sun Mingqing, Wang Yingjun. Experimental studies on SHCC pipe with FRP as lining and reinforcement under three-edge bearing test[J]. Journal of Huazhong University of Science and Technology(Natural Science Edition), 2017, 45(5): 127–132.[胡继洪，孙明清，王应军 .FRP SHCC 管道三边支撑受压试验研究[J]. 华中科技大学学报(自然科学版), 2017, 45(5): 127–132.]

[11] Hu Jihong, Sun Mingqing, Huang Wei, et al. Debonding failure in FRP reinforced SHCC beams induced from multiple flexural-shear cracks under three-point bending test[J]. Computer Modeling in Engineering & Sciences, 2021, 127(1): 191–207.

[12] Chen Jianfei, Teng Jinguang. Anchorage strength models for FRP and steel plates bonded to concrete[J]. Journal of Structural Engineering, 2001, 127(7): 784–791.

[13] Teng J G, Smith S T, Yao J, et al. Intermediate crack-induced debonding in RC beams and slabs[J]. Construction and Building Materials, 2003, 17(6/7): 447–462.

[14] American Concrete Institute. Guide for the design and construction of externally bonded FRP systems for strengthening concrete structures: ACI 440.2R—2008[S]. Farmington Hills: American Concrete Institute, 2008.

[15] Lu Xinzheng. Study on interface behavior of FRP – concrete[D]. Beijing: Tsinghua University, 2005.[陆新征 .FRP–混凝土界面行为研究[D]. 北京：清华大学, 2005.]

[16] Cohen M. Numerical analysis of debonding mechanisms of externally bonded FRP reinforcement in RC beams[D]. Waterloo: University of Waterloo. 2018.

[17] Al–Saawani M A, Al–Negheimish A I, El–Sayed A K, et al. Finite element modeling of debonding failures in FRP-strengthened concrete beams using cohesive zone model [J]. Polymers, 2022, 14(9): 1889.

[18] Teng Jinguang, Yuan Hong, Chen Jianfei. FRP-to-concrete interfaces between two adjacent cracks: Theoretical model for debonding failure[J]. International Journal of Solids and Structures, 2006, 43(18/19): 5750–5778.

[19] Wang Jialai. Cohesive zone model of intermediate crack-induced debonding of FRP-plated concrete beam[J]. International Journal of Solids and Structures, 2006, 43(21): 6630–6648.

[20] Chen Fangliang, Qiao Pizhong. Debonding analysis of FRP-concrete interface between two balanced adjacent flexural cracks in plated beams[J]. International Journal of Solids and Structures, 2009, 46(13): 2618–2628.

[21] Xu Rongqiao, Liu Cheng. CZM-based debonding simulation of cracked beams strengthened by FRP sheets[J]. Journal of Engineering Mechanics, 2012, 138(2): 210–220.

[22] Slaitas J, Valivonis J, Juknevičius L, et al. Load-bearing capacity of flexural reinforced concrete members strengthened with fiber-reinforced polymer in fracture stage[J]. Advances in Mechanical Engineering, 2018, 10(5): 1–16.

[23] Razaqpur A G, Lamberti M, Ascione F. Debonding evolution in nonlinear FRP-retrofitted RC beams with cohesive interface[J]. Composite Structures, 2020, 236: 111858.

[24] Xie Jianhe, Huang Kunhong, Guo Yongchang, et al. Energy release rate of interface crack in rc beams strengthened with fiber reinforced polymer under four point bending[J]. Poly-

mers and Polymer Composites,2014,22(8):661–668.
[25] Maalej M, Li V C. Flexural/tensile-strength ratio in engineered cementitious composites[J]. Journal of Materials in Civil Engineering,1994,6(4):513–528.
[26] Niu Hedong, Karbhari V M, Wu Zhishen. Diagonal macrocrack induced debonding mechanisms in FRP rehabilitated concrete[J]. Composites Part B: Engineering, 2006, 37(7/8): 627–641.
[27] Japan Society of Civil Engineers. Recommendations for design and construction of high performance fiber reinforced cement composite with multiple fine cracks[R]. Tokyo: Japan Society of Civil Engineer,2007.
[28] Rebecca J G. Non-linear overload behaviour and ductility of reinforced concrete flexural members containing 500 MPa grade steel reinforcement[D]. Australia:Adelaide University,2002:57–61.
[29] Li Jun. Mechanical properties of strain hardening cement-based composites and structural analysis of their pipes[D]. Wuhan: Wuhan University of Technology,2017.[李俊. 应变硬化水泥基复合材料的力学性能及其管道的结构分析[D]. 武汉:武汉理工大学,2017.]
[30] Nakaba K, Toshiyuki K, Tomoki F, et al. Bond behavior between fiber-reinforced polymer laminates and concrete[J]. ACI Structural Journal,2001,98(3):359–367.

Debonding Analysis Model and Experimental Investigations on FRP Plates Reinforced SHCC Beams Under Three-point Bending

HU Jihong, *SUN Mingqing**, *WANG Yingjun*, *CHEN Jianzhong*, *HUANG Wei*

(Hubei Key Laboratory of Theory and Application of Advanced Materials Mechanics, Wuhan University of Technology, Wuhan 430070, China)

Abstract:

Objective Strain-hardening cement-based composites (SHCC) exhibit inherent characteristics of multiple microcracking under uniaxial tension and bending, which reduces stress concentration at the crack mouth and delays debonding failure between SHCC and externally bonded FRP plates during the bending of FRP plate-strengthened SHCC beams. This study conducts experimental investigation and theoretical analysis on SHCC beams reinforced with externally bonded FRP plates to examine their debonding behavior, providing guidance for the engineering application of such structural systems.

Methods The mechanical model based on composite beam theory was developed by satisfying the requirements of force equilibrium and strain compatibility while simultaneously allowing for interfacial partial slip at the FRP-concrete interface. The theoretical analysis included two loading stages: before SHCC cracked and after SHCC cracked. Before SHCC cracked, SHCC and FRP were treated as Euler–Bernoulli beams and were connected based on reasonable interface rules; the interfacial shear stress was then obtained using the linear elastic mechanics method. After SHCC cracked, to quantify the effect of SHCC multiple fine cracks on interfacial bond stress, segmental stiffness reduction was conducted based on the moment-curvature relation, which combined interface stress analysis and equations on sectional internal force balance to construct the mechanical analysis model. First, the cracked FRP–SHCC beams were divided into two parts: the elastic part and the SHCC cracked part. Then, the SHCC cracked part was subdivided into several segments. Second, the bending stiffness and the height of the compression zone of SHCC at the joint between the elastic zone and cracked zone and at midspan were obtained by solving the equilibrium equation of the cross-section force system. Third, the bending stiffness and the height of the compressive zone of each segment were assumed to change linearly from the midspan to the elastic part. Finally, the simplified linear interface bond-slip relation, the constitutive relations of FRP and SHCC, and the control differential equations on the axial force of FRP were utilized to establish the analysis model for FRP-reinforced SHCC beams. The solution was programmed using MATLAB software. Three-point bending tests of FRP–SHCC beams with different geometric dimensions and different FRP thicknesses were performed to verify the validity of the analysis model. Single-side shear tests on the FRP–SHCC interface were performed to obtain the interfacial bond stress-slip relationship. The typical interface bond stress-slip curve included an ascending branch and a descending branch, which was similar to that of the FRP–RC interface. Based on the fine finite element analysis by Lu et al., the interfacial shear stress near the crack zone exhibited a highly brittle descent after reaching its peak value. Further studies showed that the calculated results were only 3.7% lower than the test results when the curve with only the ascending branch was applied to the whole beam. The bond stress-slip relationship indicated by Lu et al. was a curve, and the shear stress dropped sharply to 0 after reaching the peak value. This study simplified the ascending curve to a straight line to simplify the calculation

Results and Discussions The deviations of the calculated peak load from the test values were in the range of −7.79% to 7.45%, the deviations of the calculated FRP strain from the test values were in the range of −11.52% to 8.13%, and the deviations of the calculated mid-span deflection from the test values were in the range of −7.33% to −22.03%. The calculation results showed that the tensile strain of FRP decreased linearly from the mid-span to the support during the elastic stage, and after the SHCC cracked, the distribution of FRP strain from the mid-span to the beam end

indicated that its decreasing rate transitioned from slow to fast and then to slow. The strain of FRP did not reach its fracture strain, which implied that the failure of the composite beams was not due to the strength failure of FRP. The calculated deformation-load curve of the FRP-SHCC beam showed that the elastic stage was short, and the slope of the curve gradually decreased with the increase of the load, indicating that the stiffness of the composite beam gradually decreased as the crack opening of the SHCC increased. The calculated mid-span deflection results aligned with the test results for most of the loading process, except for a short segment near the peak load. In the test, when approaching the peak load, the slope of the load-deformation curve gradually decreased, indicating the occurrence of interface debonding. It was likely that the linear interface bonding stress-slip relationship adopted in the model used in this study could not reflect this process, which remained an issue requiring further investigation. The slope of the FRP strain-load relationship curve significantly decreased when the SHCC initially cracked and then approached a constant. The slope of the curve was also larger when the thickness of the FRP plate increased. The calculated values were in reasonable agreement with the test results. The calculated interface shear stress showed that during the elastic stage, the interfacial shear stress gradually increased from mid-span to the plate end. After the SHCC cracked, the interfacial shear stress first increased and then decreased from mid-span to the end of the plate. The interface shear stress reached its maximum at a position corresponding to the height of the beam from the mid-span, initiating FRP debonding. These results were consistent with the phenomena observed in the test.

Conclusions This study quantifies the process of crack opening and development in different regions of cracked SHCC through segmental stiffness reduction, and the debonding failure load of FRP-reinforced SHCC beams is determined by combining internal force balance equations with interface stress analysis. The results showed reasonable agreement with the experimental data, indicating that the approach can be applied to the analysis of this type of new civil engineering structure.

Key words: FRP plates reinforced SHCC beams; debonding; beam segment; bending stiffness; interface; bond stress

（编辑　张　琼）

引用格式: Hu Jihong,Sun Mingqing,Wang Yingjun,et al.Debonding analysis model and experimental investigations on FRP plates reinforced SHCC beams under three-point bending[J].Advanced Engineering Sciences,2025,57(4):208–217.[胡继洪，孙明清,王应军,等.三点弯曲下FRP板增强SHCC梁的剥离分析模型与试验研究[J].工程科学与技术,2025,57(4):208–217.]